J Mater Sci (2007) 42:1162–1168
DOI 10.1007/s10853-006-1445-1

Effects of fiber orientation on the acoustic emission and fracture characteristics of composite laminates

Nak-Sam Choi · Sung-Choong Woo · Kyong-Yop Rhee

Received: 17 November 2005 / Accepted: 2 May 2006 / Published online: 14 January 2007

Abstract The effects of fiber orientation on acoustic emission (AE) characteristics have been studied for various composite laminates. Reflection and transmission optical microscopy were used to investigate the damage zone of specimens. AE signals were classified through short time Fourier transform (STFT) as different types: AE signals with a high intensity and high frequency band were due to fiber fracture, while weak AE signals with a low frequency band were due to matrix cracking and/or interfacial cracking. Characteristic feature in the rate of hit-events having high amplitudes showed a procedure of fiber breakages, which expressed the characteristic fracture processes of notched fiber-reinforced plastics with different fiber orientations. As a consequence, the behavior of fracture in the continuous composite laminates could be monitored through nondestructive evaluation (NDE) using the AE technique.

N.-S. Choi (✉)
Department of Mechanical Engineering, Hanyang University, 1271, Sa-1dong, Ansan-si, Kyunggi-do 426-791, Korea
e-mail: nschoi@hanyang.ac.kr

S.-C. Woo
Department of Mechanical Design, Graduate School, Hanyang University, 17, Haengdang-dong, Sungdong-ku, Seoul 133-791, Korea

K.-Y. Rhee
School of Mechanical and Industrial System Engineering, Kyunghee University, Yongin 449-701, Korea

Introduction

Fiber-reinforced plastic composites (FRPC) have been extensively used in the aerospace industry, automobile industry, sports utilities, electronic industry and architecture due to their advantages of superior strength-to-weight and stiffness-to-weight. Damage occurrence in composite materials under in-use conditions may, however, reduce their mechanical performance. Thus, the fracture behavior of composite materials has often been examined with the aid of acoustic emission (AE) non-destructive evaluation methods to get useful information in order to improve their structural integrity and reliability.

Using single-fiber-reinforced and short-fiber-reinforced composites, many researchers [1–3] reported on the correlation of AE data with the individual fracture processes of FRPC although the fracture processes were rather complex: Fiber fracture was liable to emit strong waves with high-frequency bands of 250–450 kHz. Matrix fracture, as well as debonding and/or friction between fibers and matrix, might generate weak waves with low-frequency band. For safety estimation of FRP tanks/vessels, ASTM standards [4, 5] recommends an evaluation based on high-amplitude AE events since those events are often indicative of the major structural damage associated with fiber breakages. The present author [6, 7] investigated short fiber reinforced thermoplastic (SFRP) composites by utilizing the frequency analysis with band-pass filters, and proposed an experimental model for AE characteristics of the stable fracture process of SFRP: AE characteristics were largely affected by the initial notch-tip radius which was influential in the damage initiation and fracture processes. It was shown

for the SFRP composites that fiber breakage ahead of the notch tip was a pre-requisite for the initiation of the main crack. The present author [8] also reported a technique for monitoring the individual fracture processes of cross-ply FRP laminates by using the classification of thermo-acoustic emissions.

In this work, we study the fracture processes of typical FRP laminates with continuous fiber reinforcement on the basis of acoustic emission characteristics. For microscopic examination and identification of fracture mechanisms in FRPC, the petrographic thin sectioning technique employing lapping and polishing of both sides of a sample [9] is utilized in combination with a fracture surface observation. This work focuses on the effects that different kinds of fiber arrangement have on AE characteristics in conjunction with the fracture processes of notched FRPC.

Experimental

Composite materials

Glass-fiber/epoxy laminates with lay-ups of $[0^0_8]_S$, $[90^0_8]_S$ and $[+45^0_4/-45^0_4]_S$ as well as satin-weave (SW) glass-fabric/epoxy laminates with lay-ups of $[0^0_4/90^0_4]_S$ and $[+45^0_4/-45^0_4]_S$. were adopted for this study. Unidirectional (UD) glass fiber/epoxy resin prepreg and (SW-$[0^0/90^0]_{16}$) glass-fabric/epoxy prepreg produced by SK Chemicals were used to manufacture the laminate specimens with a thickness of 2–2.5 mm. They were made in autoclave using a curing cycle recommended by the manufacturer. Flat-type specimens 15 mm wide and 180 mm long were made by sectioning the laminates using a diamond wheel cutter. Specimen length directions were kept parallel with the fibers for the laminate UD-$[0^0_8]_S$ and perpendicular to the fibers for the laminate UD-$[90^0_8]_S$, and transverse to the fabric structures for the satin-weave laminate (SW-$[0^0/90^0]_{16}$). The gauge portion had a single-edge notched with a low speed diamond wheel cutter. The notching direction was perpendicular to the specimen length. After that, a sharp notch was introduced by pushing a fresh razor blade with a static load of 300 N into the initial notch tip. The notch depth was kept to 7.5 ± 0.2 mm.

Acoustic emission measurement

Tensile tests with a cross-head speed of 0.1 mm/min were performed. Five specimens were tested for each kind of composite. To monitor the fracture processes of the specimens, AE measurement data was recorded in real time using a two-channel AE detection system (MISTRAS 2001, PAC). AE waves were detected by two transducers (micro30, PAC) having similar sensing characteristics (100–600 kHz with peak sensitivity at 275 kHz). The two sensors were mounted on one side of the specimen (see S_1 and S_2 in Fig. 1) using vacuum grease and mechanical fixtures. The distance between the two transducers and the initial notch tip was kept to 10.0 ± 0.2 mm. AE measurement conditions of preamp 40 dB and a threshold level of 40 dB were adopted.

The AE detection system determined source locations of AE waves based on timed data of wave arrival at the transducers S_1 and S_2, and on a preset wave velocity. To measure the arrival time difference the clock rate was 4 MHz. Pencil lead (dia. 0.5 mm, lead length 3 mm, HB) breakage was used as a simulated AE source for the measurement of the wave propagation velocity in the direction of specimen length. The velocity was obtained through confirmation of the source location so that the output location could be detected accurately from the original location of input lead breaks. Figure 2 shows the results of AE wave velocity measured for the respective specimens. Values of the wave propagation velocity for each specimen were on a level with the Lamb wave velocity

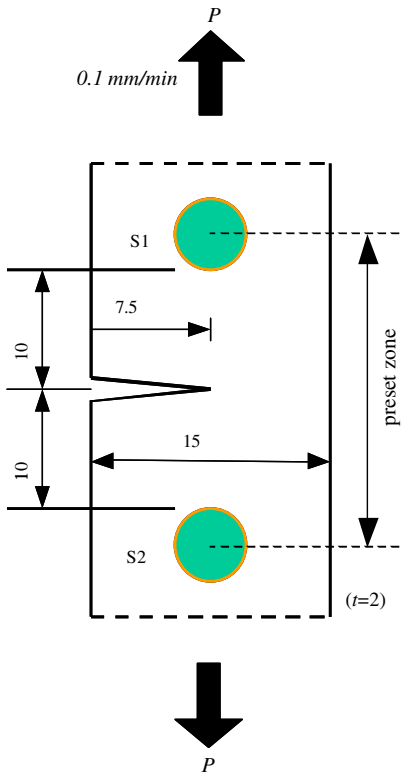

Fig. 1 Notched specimen of composite laminates and AE sensor locations S1 and S2

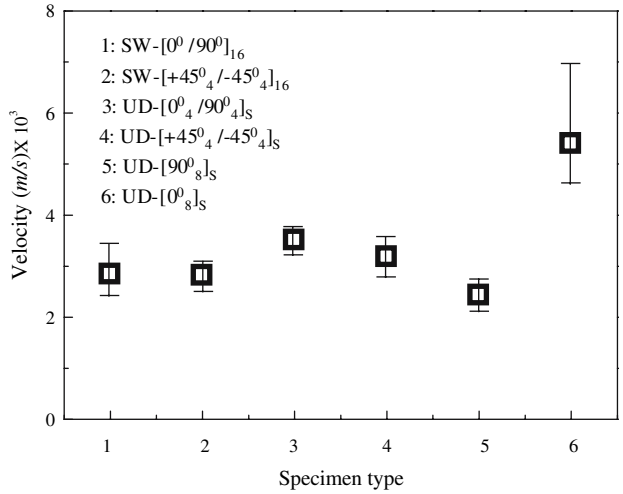

Fig. 2 Measurement results of AE propagation velocity depending on lay-ups of composite laminates

dominantly corresponding to the transverse wave velocity calculated in consideration of the elastic modulus of the corresponding specimen.

For real AE measurement, AE signals coming from outside of the pre-set zone between transducers were disregarded as noises.

Fiber orientation effects of AE characteristics and discussions

For a UD-$[90^0_8]_S$ composite specimen, a typical load P-displacement δ curve and accompanying histograms of the AE hit-event rate are shown in Fig. 3. A blast type of AE waves with low and intermediate amplitudes in a range of 40–70 dB were adopted as hit-events in this figure. Each histogram of the event-rate shows the number of events obtained during a measurement time of 3 s intervals. Detectable AE events began to occur at a displacement of 0.14 mm and corresponded to about 63% of the maximum load P_{max}. As δ increased further up to the P_{max} point corresponding to the crack initiation point, the event rate showed an increase with irregular variations (see stage I in Fig. 3). Just after the crack initiation, the load abruptly dropped due to the rapid crack propagation revealing a drastic rise in the event rate (see the early portion of stage II). With increasing displacement in the next portion of stage II, the load gradually decreased due to the slow crack growth. This cracking process showed a decrease in the average event-rate, which might be indicative of a decrease in the size of the damage zone formed during each unit length of displacement. Using the short time Fourier transform, it was confirmed that most of the AE hit events had a low frequency band of 40–270 kHz as shown in Fig. 4. Thus those AE events are considered to have occurred due to matrix fracture, fiber-matrix interfacial failure and pull-out process of fibers as reported in references [2, 3, 6, 7].

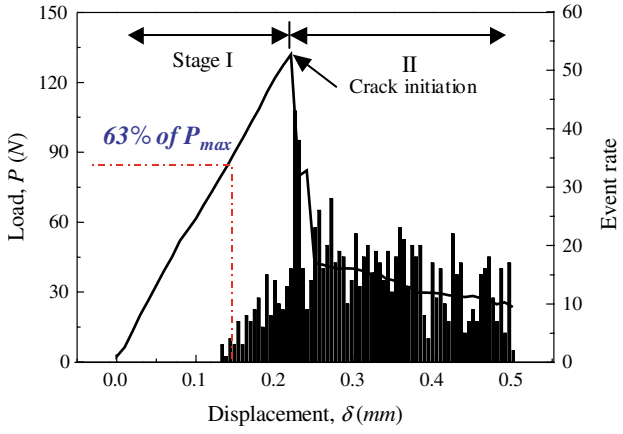

Fig. 3 Typical diagrams of load P and AE event rate versus displacement δ for unidirectional $[90^0_8]_S$ composite specimen: accompanying AE event rate data was obtained from signals with low and intermediate amplitudes from 40 to 70 dB

Figure 5 shows histograms of the event rate in a high amplitude range beyond 70 dB for the same specimen in Fig. 3. Over 90% of AE events processed by the short time Fourier transform was shown to have both high and low frequency bands of 40–480 kHz (see Fig. 6), suggesting emissions from the fiber breakage and accompanying matrix fracture [1–3, 6, 7]. Thus the hit-events behavior may represent the histories of fiber breakages during the fracture processes of the individual composites. The reason why hit-events were hardly measured in stage I before the crack initiation point, P_{max}, may be that few fibers were broken in front of the initial crack tip under the transverse tensile loading. A further increase of δ into the stage II past the P_{max} point brought about a large amount of hit-event rate during the crack growth. This AE activity seemed to be due to the breakages of fibers which had been bridged

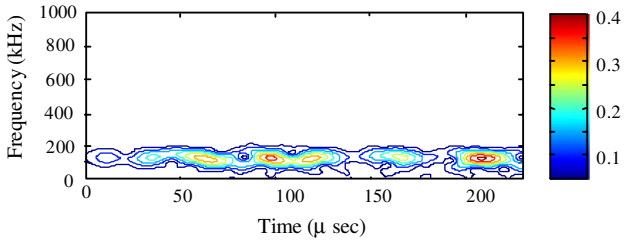

Fig. 4 A weak AE signal processed by the short time Fourier Transform with low frequency bands

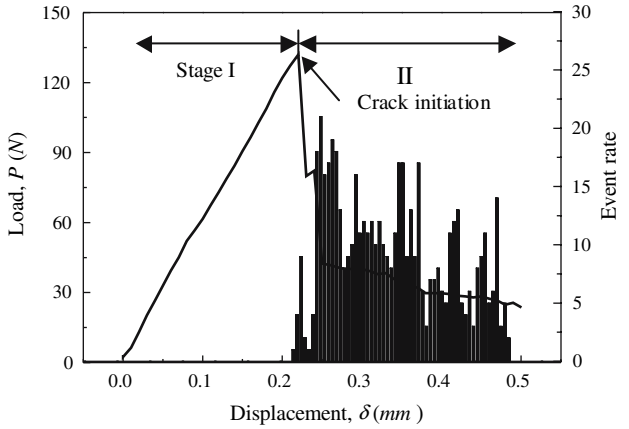

Fig. 5 Typical diagrams of load P and AE event rate versus displacement δ for the same specimen as used in Fig. 3: accompanying AE event rate data was obtained from signals with high amplitudes beyond 70 dB

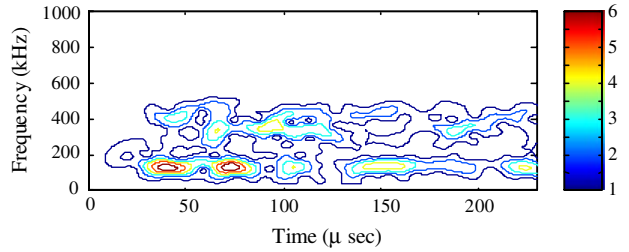

Fig. 6 A strong AE signal processed by the short time Fourier Transform, showing a blast-type wave with both high and low frequency bands

across the upper and lower crack surfaces behind the crack tip (see broken fibers on the fracture surface in Fig. 7).

For notched UD-$[0^0{}_8]_S$ unidirectional composite specimens, a typical P-δ curve and accompanying histograms of event rate in the high amplitude range

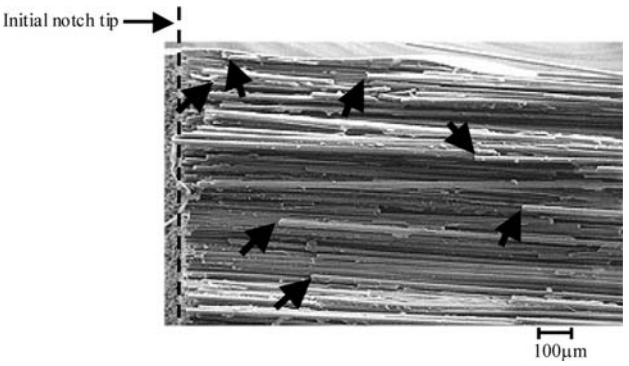

Fig. 7 Scanning electron microscopy observation of the fracture surface of the specimen of Figs. 3 and 5. Arrows indicate broken fibers produced during the crack propagation

are presented in Fig. 8. With a very high strength 46 times larger than that of UD-$[90^0{}_8]_S$ specimen, the UD-$[0^0{}_8]_S$ specimen showed the maximum event rate around δ = 2.3 mm. However, a drastic decrease in the event rate to a minimum was obvious at δ = 2.6 mm corresponding to about 72% of P_{max} (see A in Fig. 8). After that, the event rate showed irregular increases with jumps up and down. With further increase of P beyond 82% of P_{max} (see B in Fig. 8), the rate rapidly decreased again to a very low level which was similar to that of UD-$[90^0{}_8]_S$ specimen shown in Fig. 5. Reflected optical observation (see Fig. 10) of the specimen in the stage of load slightly below 82% P_{max} showed that many fiber breakages took place ahead of the initial notch tip, which corresponded to the events arisen before A. Crack advance became totally shifted to a 90° angle parallel to the fiber orientation, which led to the shearing mode (mode II) fracture (see shear crack in Fig. 9) showing minor fiber breakages. The main crack finally propagated perpendicular to the initial notching direction. It is thought for the fracture process that at the 1st minimum point (A) in the hit-event rate, the loading state causing the mode I fracture began to change to a different state causing the approximately mode II fracture around the notch tip. The fracture mode change to shearing induced the formation of different damage zones and additional fiber breakages in the load stage between A and B. As the load passed over B, a complete mode change seemed to be accomplished together with the propagation of a shear crack causing additional fiber breakages. The AE activity in this final load stage seemed to have arisen from the breakage of fibers, which had been bridged across the

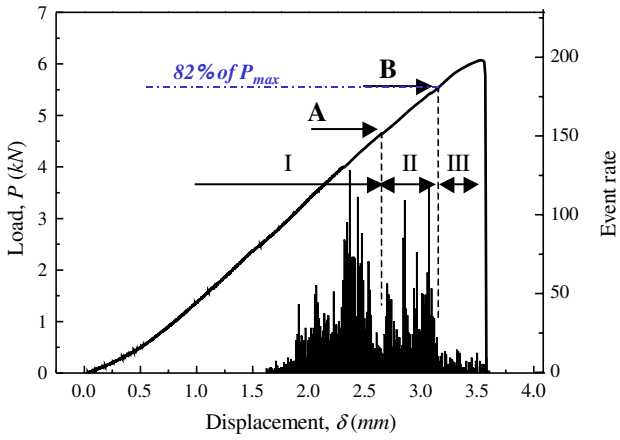

Fig. 8 Typical diagrams of load P and AE event rate versus displacement δ for $[0^0{}_8]_S$ composite specimen: accompanying AE event rate data was obtained with high amplitudes beyond 70 dB

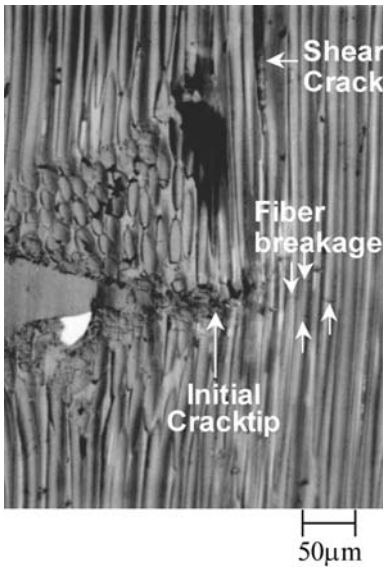

Fig. 9 Reflected optical micrograph of notched UD-$[0^0_8]_S$ specimen in load stage II of Fig. 8

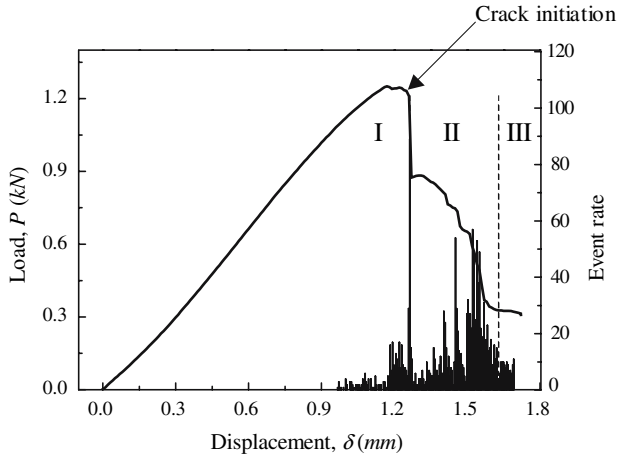

Fig. 10 Typical diagrams of load P and AE event rate versus displacement δ for $[+45^0_4/-45^0_4]_S$ composite specimen. Accompanying AE event rate data was obtained with high amplitudes beyond 70 dB

upper and lower crack surfaces behind the crack tip, as similarly observed in Fig. 5.

For cross-ply composite specimens with layup of $[+45^0_4/-45^0_4]_S$, the event rate in the high amplitude range increased greatly as the load approached the maximum (see stage I in Fig. 10). This might be on account of fiber breakages in front of the initial crack. Just after passing the maximum load, a large load drop with a very high event rate arose due to the existence of rapid crack propagation. The cracking progressed parallel to the fiber length direction in the skin and core layers, i.e. at +45° or –45° angles to the notching. During this process, a substantial number of fibers hindering the crack advance were broken, which generated the high event rate. In the beginning of stage II shortly after that, the cracking was arrested on account of large hindrance effects by crossed fibers in the neighboring layers. As δ increased further in stage II, the event rate was temporarily minimized before rapidly increasing again. This behavior of the event rate exhibiting irregular jumps up and down may indicate that the cracks advanced further inducing additional fiber breakages and various partial delaminations between layers.

Figure 11 shows a typical P–δ curve and accompanying histograms of the AE hit-event rate in the high amplitude range for a SW-$[0^0/90^0]_{16}$ specimen. AE event rate data was obtained from high amplitude signals beyond 70 dB. The behavior of the AE amplitude distribution for the specimen of this figure is exhibited in Fig. 12. A value of 0 μV in peak amplitude in this figure corresponded to 40 dB. Around $\delta \fallingdotseq 0.62$ mm, the maximum hit-event rate was observed with the generation of an AE wave having one of the biggest amplitudes. Then it decreased to a minimum at $\delta \fallingdotseq 0.66$ mm, where a considerable decrease in the amplitude was also ascertained. At this displacement corresponding to about 92% of P_{max}, it could be observed using a traveling microscope that the main crack was initiated. A thin polished section with a thickness of about 60 μm obtained from a different satin weave $[0^0/90^0]_{16}$ specimen loaded to 92% P_{max} was examined under polarized light. After observing the transmitted light image of Fig. 13b, it was confirmed that many fiber breakages were obvious in front of the main crack initiation site seen in the reflected light image of Fig. 13a. The main crack under

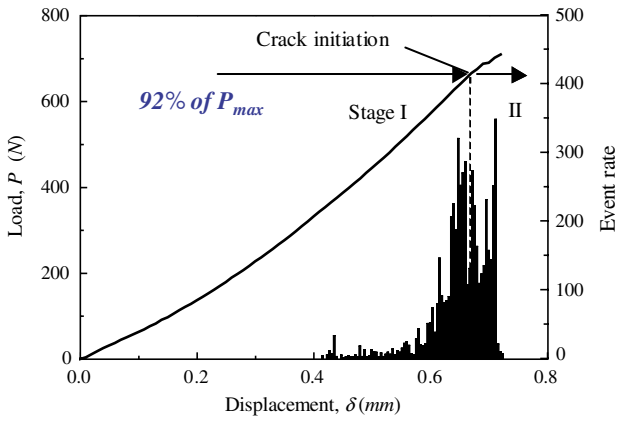

Fig. 11 Typical diagrams of load P and AE event rate versus displacement δ for a satin weave $[0^0/90^0]_{16}$ composite specimen. AE event rate data was obtained from high amplitude signals beyond 70 dB

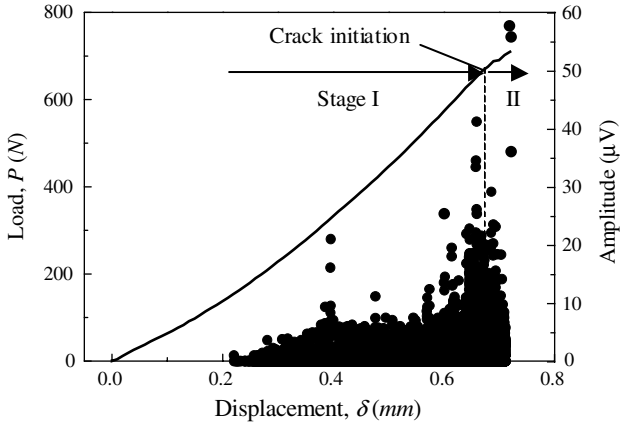

Fig. 12 Behavior of the AE amplitude distribution versus δ for the specimen of Fig. 11. The amplitude data was obtained from all AE signals beyond the threshold level (40 dB)

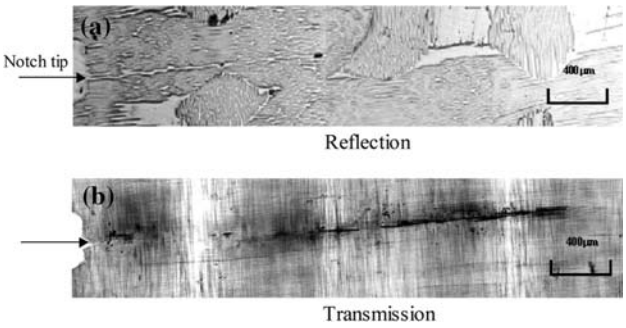

Fig. 13 Polarized optical microscopy observation of fracture processes in a satin-weave composite specimen: (**a**) and (**b**) micrographs were taken from a thin section with a thickness of about 60 μm under reflected and transmitted light, respectively. The section had been made after loading the specimen to about 92% of P_{max}. Many fiber breakages were obvious in front of the initial notch tip

tensile loading followed the rather straight-forward pathway spanned by reinforcing fibers in front of the initial notch tip, which induced breakages of the fibers

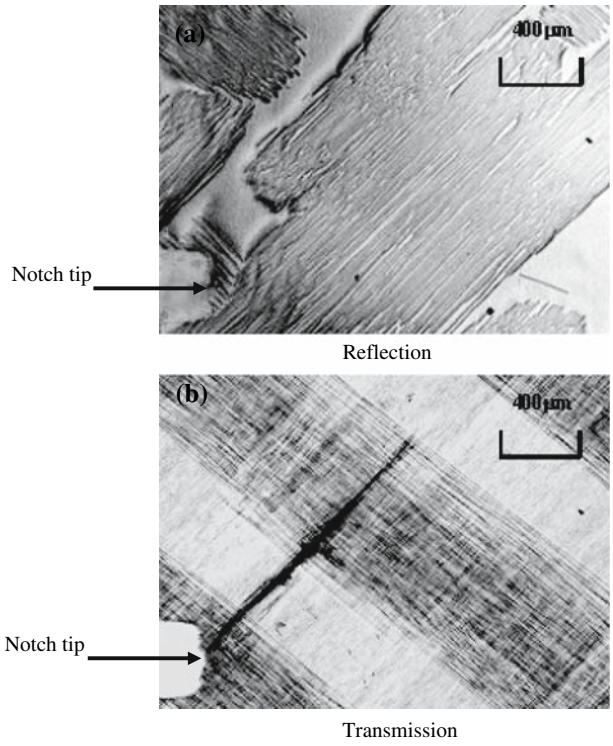

Fig. 14 Polarized optical microscopy observation of fracture processes in a satin-weave -$[+45^0/-45^0]_{16}$ composite specimen around 95% of P_{max}: (**a**) and (**b**) micrographs were taken from a thin section with a thickness of about 100 μm under reflected and transmitted light, respectively

hindering the crack initiation. Considering that the hit-events with high amplitudes were generated due to fiber breakages, it is understandable also in stage I of Figs. 11 and 12 that fiber breakages ahead of the initial notch tip led to the initiation of the main crack. This result was similar to that of references [6, 7] based on short-fiber-reinforced plastics in that fiber breakages were a pre-requisite for the main crack initiation. During main crack propagation, additional fiber breakages occurred depending on the extent of the local

Table 1 Fracture process and AE characteristics for notched composites

	Fracture process	AE
UD-$[0^0_8]_S$	1. Main crack initiation	Minimized amplitude and event rate similar to the results of ref. [6, 7]
	2. Fracture mode change	Dual peak distribution, High event rate
	3. Shear crack propagation	Low event rate
UD-$[90^0_8]_S$	1. Until crack initiation	Few AE
	2. Crack propagation	Low event rate
UD-$[+45^0_4/-45^0_4]_S$	1. Until crack initiation	Low amplitude, Low event rate
	2. Crack propagation and delamination	Low and high amplitudes, High event rate
SW-$[+45^0/-45^0_4]_{16}$	1. Main crack initiation	Minimized amplitude and event-rate, Dual peak distribution similar to the results of ref. [6, 7]
	2. Crack propagation	Increased amplitudes, High event rate
SW-$[0^0/90^0]_{16}$	Same as above	Same as above

failure zone and caused a rapid increase in the AE event rate (see stage II in Fig. 11). This result was also similar to references [6, 7].

Similar behavior of the AE hit-event rate and the main crack initiation mechanisms were also shown for SW-$[+45^0/-45^0]_{16}$ specimens, except that the load at the crack initiation was about 95% of P_{max}, 1.8 times larger than that of SW-$[0^0/90^0]_{16}$. The main cracking was rarely visible when viewed under reflected light (see Fig. 14a). However, at this load stage some advance of matrix microfracture and many fiber breakages were seen in a 45° direction biased from the notching direction under transmitted light (see Fig. 14b) confirming the high AE activity behavior in advance of the main cracking.

Conclusions

Table 1 summarizes fiber orientation effects on the characteristic behaviors of AE hit-event rate in a high amplitude range above 70 dB for various kinds of typical composite laminates. The AE characteristics might represent the process of fiber breakages according to the various loading stages, which expressed characteristic fracture processes for individual fiber-reinforced composite laminates. The feature of the AE hit-event rate, in combination with AE amplitude classifications, could be utilized for non-destructive identification of different fracture mechanisms, which can help to better understand mechanical toughness and, thus, make more reliable design of fiber reinforced composite materials and structures.

Acknowledgement This work was supported by grant No. (R01-2005-000-10566-0) from the Basic Research Program of the Korea Science & Engineering Foundation.

References

1. Wolters J (1986) In: Proceedings of 2nd international symposium on AE from reinforced composites. The Society of the Plastics Industry, Montreal, pp 29–36
2. Koenczoel L, Hiltner A, Baer E (1987) Polym Compos 8:109
3. Suzuki M, Nakanishi H, Iwamoto M, Jinen E, Maekawa Z, Koike K (1987) J Soc Mater Sci Jpn 36:229
4. Standard practice for acoustic emission examination of reinforced thermosetting resin pipe (RTRP), ASTM Designation: E1118-00. American Society for Testing and Materials, West Conshohocken, PA, (December 2000)
5. Standard practice for acoustic emission examination of fiberglass reinforced plastic resin (FRP) Tanks/Vessels, ASTM Designation: E1067-01. American Society for Testing and Materials, West Conshohocken, PA, (July 2001)
6. Choi NS, Takahashi K, Hoshino K (1992) NDTE Int 25:271
7. Choi NS, Takahashi K (1998) J Mater Sci 33:2357
8. Choi NS, Kim YB, Kim TW, Rhee KY (2003) J Mater Sci 38:1013
9. Choi NS, Takahashi K (1993) J Mater Sci Lett 12:1718